8 (3): 206-213 (2024)

Journal of Aviation

https://dergipark.org.tr/en/pub/jav

e-ISSN 2587-1676

Maximization of Flight Performance of Eight-Rotor Multirotor with Differentiated Hub Angle

Enes Özen[1*], Tuğrul Oktay[2]

[1*]Hasan Kalyoncu University, Mechanical Engineering Department, Gaziantep, Türkiye. (enes.ozen@hku.edu.tr)
[2] Erciyes University, Aircraft Engineering Department, Kayseri, Türkiye. (oktay@erciyes.edu.tr)

Article Info

Received: 27 May 2024
Revised: 02 September 2024
Accepted: 07 September 2024
Published Online: 06 October 2024

Keywords:
Morphing Multirotor
PID
SPSA
Flight Performance

Corresponding Author: *Enes Özen*

RESEARCH ARTICLE

https://doi.org/10.30518/jav.1490356

Abstract

The aim of this article is to design a rotary wing aircraft autopilot system that improves flight performance by changing the body shape during flight. The method is to obtain values that stabilize the longitudinal and lateral flight of the aircraft, where the amount of metamorphosis and Proportional-Integral-Derivative (PID) coefficients are determined using the simultaneous perturbation stochastic approximation (SPSA) optimization algorithm. The rotary wing aircraft has a deformable structure with eight rotors. Shape-changing rotary-wing aircraft are aircraft that can fly with the lift generated by propellers. Aerial platform; It consists of arms and trunk. The angle between mechanism A and the arm to which the rotors are connected can be changed with the horizontal plane and different configurations are obtained. When the angle between the arms is 45°, the octo configuration turns into a stable structure, while when the angle between the arms is 0°, the X8 configuration provides high maneuverability and increased controllability. Metamorphosis, its effect on longitudinal and lateral flight stability and improvement studies were carried out in a simulation environment and the results are presented in this study. As a result of the shape change, longitudinal and lateral narrowing occurred by 26.8° percent. Simulation tests were modeled in a closed environment, free from atmospheric effects. The obtained flight performance values are presented in Tables.

1. Introduction

Unmanned aerial vehicle (UAV) is an unmanned or remote-controlled aircraft (Bao et al., 2022). UAVs are generally used in various fields such as reconnaissance, surveillance, mapping, security, and agriculture (Husain et al., 2022). UAVs can be produced in different sizes and shapes. Small-sized UAVs are hand-held devices with cameras and various sensors (Chen et al., 2022). Larger-sized UAVs can generally have fixed wings and can travel longer distances (Çoba et al., 2020). Rotary-wing unmanned aerial vehicle is a type of UAV that can hover and stay in the air via its rotating wings (Falanga et al. 2018). Such UAVs operate similarly to helicopters and can take off and land vertically in the air (Alanezi et al., 2022). Rotary-wing UAVs can be used in many different areas such as reconnaissance and surveillance, rescue, agriculture, firefighting, mining, construction, film production and military purposes. They are usually produced in small sizes and are portable. Some models may have different features such as cameras, thermal imagers, laser meters and other sensors. Thanks to these features, rotary-wing UAVs can perform various tasks. Rotary wing aircraft are named according to the number of rotors they have. In this study, the aircraft type with eight rotors is named in the literature as X8 and octo. Conventional quad-rotor aircraft are designed for indoor or outdoor use. While smaller volume aircraft are preferred for indoor use, the octocopter structure, which is more resistant to atmospheric disturbances, is preferred (Zhang et al., 2022). The design and optimization of an eight-rotor aircraft controller that can change shape and has a structure suitable for both situations is the subject of this study.

Optimization of morphing aircraft requires considering factors such as its design, material selection and control system to improve the performance of the aircraft and increase its energy efficiency.

The optimization process usually includes these steps:

1. Problem definition: Identifying problems such as objectives, requirements and constraints for designing the aircraft.

2. Design variations: Identifying different design options, e.g. evaluating different options such as continuous deformation technologies or modular designs.

3. Analysis and testing: Comparison of selected designs with computer simulations or real tests.

4. Optimization: Determination of the best design or combination is evaluated according to the necessary criteria to ensure the most appropriate choice in terms of performance and cost.

5. Redesign: Improving the qualities of the selected designs and redesigning them when necessary.

6. Application: Production and flight testing of the optimized morphing aircraft.

The choice of materials used in the design of the shape-shifting aircraft is also important. By using light and durable materials, energy efficiency can be increased and flight costs can be reduced. Finally, control systems must also be optimized and be able to optimize the aircraft's flight stabilizations and performance.

In this study, the simultaneous X8-octo autopilot system is considered both longitudinally and laterally. For the first time, methods of changing the arm intersection angles of an eight-rotor aircraft were combined and applied as morphing in the simulation. In order to implement the transformation, a multirotor mathematical model was created using the Newton-Euler method. Mathematical model of multirotor dynamics is developed using Newton-Euler method. Both linear and nonlinear equations are derived in mathematical model. However, linear equations are used in state space model approach. Modeling was done with a state space model approach using linear equations of motion (Debines et al.,2017). To make it more stable against longitudinal and lateral flight parameter changes, the PID control algorithm was used, and the SPSA optimization method was used to best estimate the PID coefficients and determine the transition parameters (Köse et al, 2021). Again, SPSA and this type of morphing were applied for the first time. Simulations were carried out with the calculated parameters and the longitudinal and lateral flight of the aircraft was controlled in the active transition state. With the results obtained, important data for quadrotor transformation has been obtained and it has been demonstrated that combining different transformation situations and optimization algorithms plays an important role in determining the transformation rate, and it is aimed to eliminate the gap in this regard.

2. Materials and Methods

2.1. Theoretical Background and Experimental Method

Unmanned aerial vehicles (UAVs) are aircraft that possess autonomous flight capabilities. These capabilities are predominantly dependent on an autopilot system, which comprises a combination of software and hardware components. The autopilot system allows UAVs to execute operations in accordance with a pre-established flight plan.

Autopilot systems enable UAVs to control various flight parameters, including altitude, speed, heading, orientation, and other critical factors. These systems process data received from the UAV's sensors and make the necessary adjustments to stabilize the flight and ensure adherence to a predefined flight plan. The autopilot system comprises numerous components, including sensors such as inertial measurement units (IMUs), GPS, airspeed sensors, barometers, and magnetometers. Additionally, hardware components like motors, propellers, and control surfaces are utilized to manage the UAV's movement. The X8-Octo model, depicted in Fig. 1, features eight propellers and corresponding rotors. The rotation directions of the rotors are provided for both configurations.

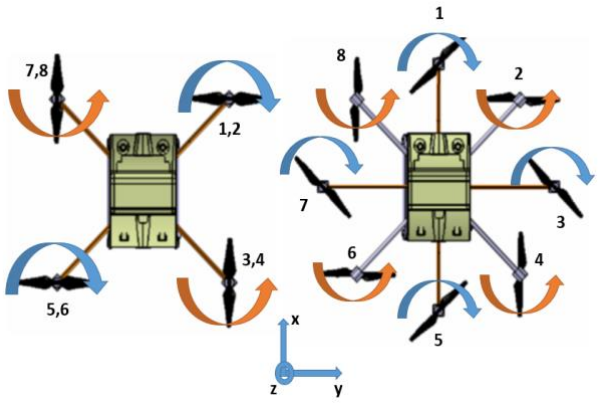

a) b)

Figure 1. a) X8 Configuration, b) Octo Configuration

The development of unmanned aerial vehicles (UAVs) has seen a significant rise, particularly in applications that require stability, precision, and versatility. An octocopter, a UAV with eight rotors, provides enhanced lift, stability, and redundancy compared to quadcopters and hexacopters. This article details the mathematical modeling of an octocopter, covering its kinematics, dynamics, rotor forces, and control systems.

Coordinate System and Notation

Inertial Frame (Earth Frame)

The inertial frame, or Earth frame, is fixed and serves as a reference:

Axes: $\{X_E, \quad Y_E, \quad Z_E\}$

Position Vector: $r_E = [x_E, \quad y_E, \quad z_E,]^T$

Body Frame (UAV Frame)

The body frame is fixed to the UAV's center of mass:

Axes: $\{X_B, \quad Y_B, \quad Z_B\}$

Position Vector: $r_B = [x_B, \quad y_B, \quad z_B,]^T$

Transformation Matrix

To transform vectors between frames, the rotation matrix R_B^E is used:

$$R_B^E = \begin{bmatrix} c\psi c\theta & c\psi s\theta s\phi - s\psi c\phi & c\psi s\theta s\phi + s\psi s\phi \\ s\psi c\theta & s\psi s\theta s\phi + c\psi c\phi & s\psi s\theta c\phi - c\psi s\phi \\ -s\theta & c\theta s\phi & s\theta s\phi \end{bmatrix} \quad (1)$$

Where ϕ, θ, and ψ represent roll, pitch, and yaw, respectively.

Kinematics

Position and Velocity

The position and velocity vectors in the inertial frame are given by:

Position Vector: $r_E = [x, \quad y, \quad z]^T$

Velocity Vector: $v_E = [\dot{x}, \quad \dot{y}, \quad \dot{z}]^T$

Orientation

Orientation can be represented using Euler angles or quaternions.

Euler Angles

- Roll (ϕ), Pitch (θ), Yaw (ψ)

The angular velocity in the body frame:

$$\begin{bmatrix} p \\ q \\ r \end{bmatrix} = \begin{bmatrix} 1 & 0 & -s\theta \\ 0 & c\phi & s\phi c\theta \\ 0 & -s\phi & c\phi c\theta \end{bmatrix} \begin{bmatrix} \dot{\phi} \\ \dot{\theta} \\ \dot{\psi} \end{bmatrix} \quad (2)$$

Dynamics

Translational Dynamics

The translational motion is described by Newton's second law:

$$m\ddot{r} = F_E + mg \quad (3)$$

Where:

F_E is the net external force in the inertial frame.

$g = [0, \quad 0, \quad -mg]^T$represent gravitational force.

The thrust force F_B in the body frame is transformed to the inertial frame:

$$F_E = R_B^E F_B \quad (4)$$

Where:

$$F_B = \left[0, \quad 0, \quad \sum_{i=1}^{8} T_i\right]^T \quad (5)$$

Rotational Dynamics

The rotational dynamics are given by the Euler equations for rigid body rotation:

$$I\omega + \dot{\omega x}(I\omega) = \tau \quad (6)$$

Where:

I is the inertia matrix, $\omega = [p, \quad q, \quad r]^T, \tau$ is the torque vector.

Forces and Torques from Rotors

Thrust and Torque of Individual Rotors

For each rotor i:

Thrust Force:

$$T_i = k_T \omega_i^2 \quad (7)$$

Where ωi is the angular speed and kt is the thrust coefficient.

Torque:

$$\tau_i = k_\tau \omega_i^2 \quad (8)$$

Where $k\tau$ is the torque coefficient.

Total Thrust and Torques

Sum the contributions from all eight rotors.

$$F_B = \begin{bmatrix} 0 \\ 0 \\ \sum_{i=1}^{8} T_i \end{bmatrix}$$
$$T = \sum_{i=1}^{8} \begin{bmatrix} y_i T_i - z_i \tau_i \\ z_i T_i - x \tau_i \\ k_\tau \omega_i^2 \end{bmatrix} \quad (9)$$

Where x_i, y_i, z_i are the rotor coordinates.

Control Allocation

Distributing the desired thrust and torques among the rotors involves mapping control inputs to rotor speeds.

Control Inputs

Control inputs u_1, u_2, u_3, u_4 correspond to:

$$u_1 = k_T(\omega_1^2 + \omega_2^2 + \omega_3^2 + \omega_4^2 + \omega_5^2 + \omega_6^2 + \omega_7^2 + \omega_8^2)$$

$$u_2 = k_T l \begin{pmatrix} \omega_5^2 \frac{\sqrt{2}}{2} \cos\alpha + \omega_6^2 \frac{\sqrt{2}}{2} + \omega_7^2 \frac{\sqrt{2}}{2} \cos\alpha + \omega_8^2 \frac{\sqrt{2}}{2} \\ -\omega_1^2 \frac{\sqrt{2}}{2} \cos\alpha - \omega_2^2 \frac{\sqrt{2}}{2} - \omega_3^2 \frac{\sqrt{2}}{2} \cos\alpha - \omega_4^2 \frac{\sqrt{2}}{2} \end{pmatrix} \quad (10)$$

$$u_3 = k_T l \begin{pmatrix} \omega_1^2 \frac{\sqrt{2}}{2} \sin\alpha + \omega_2^2 \frac{\sqrt{2}}{2} + \omega_7^2 \frac{\sqrt{2}}{2} \sin\alpha + \omega_8^2 \frac{\sqrt{2}}{2} \\ -\omega_5^2 \frac{\sqrt{2}}{2} \sin\alpha - \omega_6^2 \frac{\sqrt{2}}{2} - \omega_3^2 \frac{\sqrt{2}}{2} \sin\alpha - \omega_4^2 \frac{\sqrt{2}}{2} \end{pmatrix}$$

$$u_4 = k_\tau(\omega_1^2 - \omega_2^2 + \omega_3^2 - \omega_4^2 + \omega_5^2 - \omega_6^2 + \omega_7^2 - \omega_8^2)$$

Considering the body structure of the shuttle rotor aircraft and the locations of the rotor, the control inputs are defined as follows.

The changes in the structure geometry after the resulting shape change are given in Table 1.

Table 1. Dimensions of Multirotor

Aircraft Configuration	Width (mm)	Length (mm)
Octo	1100	1100
X8	777	777

2.2. Control System

2.2.1. Hierarchical Autopilot System

The X8-Octo UAV calculates linear and angular movements using the angular and linear acceleration data obtained from its sensors. The control signal u_1 is used to control altitude, while u_2, u_3, and u_4 are employed to manage roll (ϕ), pitch (θ), and yaw (ψ) movements, respectively. Although there are four control signals, the system governs six states, rendering it underactuated (Köse et al., 2019). The four control inputs available—pitch, roll, yaw, and altitude—are used to manage these motions. To enable linear forward and lateral movements, the flight control software installed on the flight controller generates two additional commands, thereby ensuring full control of the aircraft. The flight control software integrates commands received from the guidance and navigation systems into its subsystems—angular and linear—and then transmits the corresponding output signals to the actuators. The system's schematic is presented in Fig. 2.

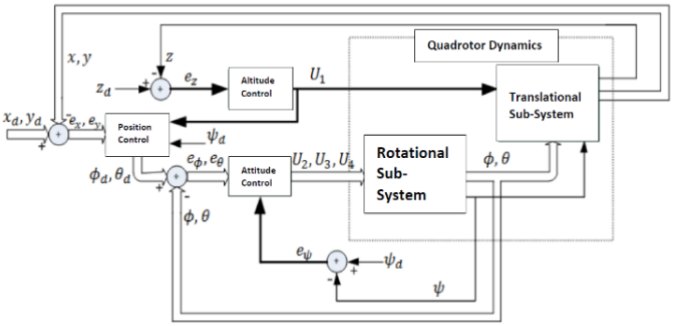

Figure 2. Hierarchical Autopilot System Structure

PID controllers manage the UAV's position and orientation. Position control for x, y, z:

$$\begin{aligned} u_x &= K_{p_x}(x_{ref} - x) + K_{d_x}(\dot{x_{ref}} - \dot{x}) \\ &\quad + K_{i_x}\int (x_{ref} - x)dt \\ u_y &= K_{p_y}(y_{ref} - y) + K_{d_y}(\dot{y_{ref}} - \dot{y}) \\ &\quad + K_{i_y}\int (y_{ref} - y)dt \\ u_z &= K_{p_z}(z_{ref} - z) + K_{d_z}(\dot{z_{ref}} - \dot{z}) \\ &\quad + K_{i_z}\int (z_{ref} - z)dt \end{aligned} \tag{11}$$

Attitude control for roll (ϕ), pitch (θ), yaw (ψ):

$$\begin{aligned} u_\phi &= K_{p_\phi}(\phi_{ref} - \phi) + K_{d_\phi}(\dot{\phi_{ref}} - \dot{\phi}) \\ &\quad + K_{i_\phi}\int (\phi_{ref} - \phi)dt \\ u_\theta &= K_{p_\theta}(\theta_{ref} - \theta) + K_{d_\theta}(\dot{\theta_{ref}} - \dot{\theta}) \\ &\quad + K_{i_\theta}\int (\theta_{ref} - \theta)dt \\ u_\psi &= K_{p_\psi}(\psi_{ref} - \psi) + K_{d_\psi}(\dot{\psi_{ref}} - \dot{\psi}) \\ &\quad + K_{i_\psi}\int (\psi_{ref} - \psi)dt \end{aligned} \tag{12}$$

This detailed mathematical model forms the basis for designing and simulating the control systems of an eight-rotor UAV. By understanding and applying these principles, we have developed more efficient, stable and robust UAV systems.

2.3. Problem Definition

Today, UAVs are employed for a wide array of purposes, ranging from applications in the entertainment industry to military operations on battlefields. The specific missions and performance requirements for UAVs vary depending on the intended use. UAVs achieve the necessary mission objectives through modifications in their geometry, a process referred to as morphing (Uzun et al., 2021). In multirotor UAVs, this morphing typically involves extending or shortening the arm length (Köse et al., 2021). However, in this study, an alternative approach is explored by altering the arm intersection angle. The geometric changes made by the X8-Octo during flight result in shifts in its dynamic properties. The key parameter affected by this morphing is the moment of inertia, as detailed in Table 2. The moment of inertia values are calculated using Eq. 13.

$$I = \frac{1}{3}ml^2 \tag{13}$$

Here l is the arm length, m is the total mass, α is the hub angle (arm intersection angle) (Fig. 3). It has two body structures of type X and + that can move independently or together. Morphing (Sal et al., 2016) is performed by changing the angle α [0°, 45°] thanks to mechanism A (Fig. 3c). The weight of each arm was considered to be one eighth of the total weight and 1 kg.

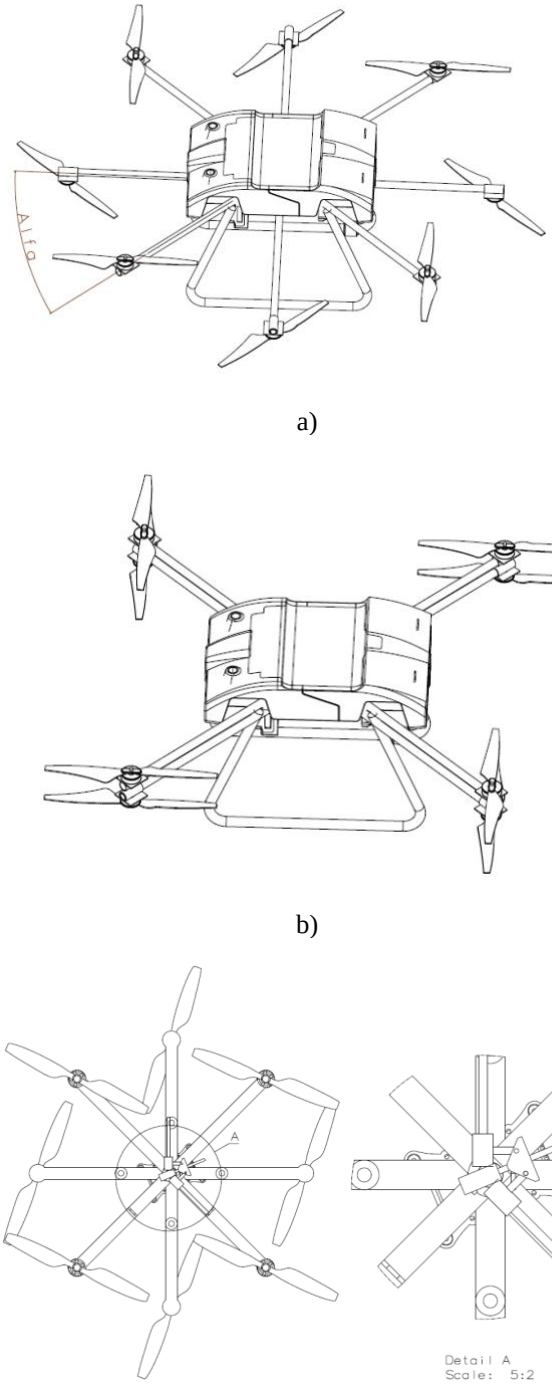

a)

b)

c)

Figure 3. a) Arm Intersection Angle (alpha=45°) b)Arm Intersection Angle (alpha=0°) c) Mechanism A

Moment during deflection; It is calculated by multiplying the moment of inertia (I_z) with respect to the z axis and the angular acceleration. Here I_z is given in Eq.14.

$$I_z = \frac{8}{3}ml^2 \tag{14}$$

The moment of inertia of the aircraft around the z-axis was calculated according to Eq.14. from Eq.3 , the moment occurring during pitching motion is calculated as I_y times the angular acceleration. Here I_y, it is obtained from Eq. 15.

$$\begin{aligned} I_{x,y} &= \frac{2}{3}m(l\cos\alpha)^2 + \frac{2}{3}m(l\sin\alpha)^2 \\ &\quad + \frac{4}{3}m\left(\frac{l\sqrt{2}}{2}\right)^2 \end{aligned} \tag{15}$$

The moment during the rolling motion is calculated as I_x times the angular acceleration. Here I_x is obtained from Eq.15.

When the angle between the arms is increased, the dynamics of the aircraft changes. According to 11 and 12, the calculation of the moments of inertia in configurations 1 and 2 is given in Eq. 14 and 15. The moment of inertia results obtained as a result of the change in shape and geometric dimensions are given in Table 2.

Table 2. Moment of Inertia Values of Eight Rotor Air Vehicles in Different Configurations

Aircraft Configuration	I_x (kgm^2)	I_y (kgm^2)	I_z (kgm^2)
Configuration 1	0.408	0.408	0.813
Configuration 2	0.408	0.408	0.813

2.3.1. SPSA Optimization Algorithm

The eight-rotor UAV in question can dynamically switch between a cross and plus configuration, providing versatility in maneuverability and stability. The transition between configurations is controlled by a hub angle, and the system's performance can be optimized by tuning 7 variable parameters, including PID coefficients for both longitudinal and lateral control. This article defines the Simultaneous Perturbation Stochastic Approximation (SPSA) optimization algorithm to optimize these parameters.

UAV Configuration

Variable Configurations

Cross Configuration (Plus Configuration): Two intersecting frames at a 45-degree angle.

X8 Quadcopter Configuration: Frames aligned at 0 degrees.

Variable Parameters

Hub Angle (α): Angle between the cross and plus configurations.

Longitudinal PID Coefficients: Kplong, Kilong, Kdlong.

Lateral PID Coefficients: Kplat, Kilat, Kdlat.

Simultaneous Perturbation Stochastic Approximation (SPSA) is an efficient method for optimizing systems with multiple parameters. It is particularly useful for systems where the objective function is noisy and the cost of evaluating the gradient is high.

SPSA Steps:
1. Initialization:
Set initial parameter values:
$\theta_0 = [\alpha, \quad K_{p_{long}}, \quad K_{i_{long}}, \quad K_{d_{long}}, \quad K_{p_{lat}}, \quad K_{i_{lat}}, \quad K_{d_{lat}}]$
Choose SPSA coefficients: a, c, A, α, γ.

Set the initial iteration count $k = 0$

2. Iteration:
For each iteration k:
Generate perturbation vector:
$\Delta_k = [\delta_\alpha, \quad \delta_{p_{long}}, \quad \delta_{i_{long}}, \quad \delta_{d_{long}}, \quad \delta_{p_{lat}}, \quad \delta_{i_{lat}}, \quad \delta_{d_{lat}}]$
Where δ_i are randomly selected from a symmetric Bernoulli distribution (±1).

Parameter perturbation:
$\theta_k^+ = \theta_k + c_k\Delta_k$
$\theta_k^- = \theta_k - c_k\Delta_k$

Objective function evaluation:
Evaluate the objective function L (e.g., cost function, error) at θ_k^+ and θ_k^- :

$L^+ = L(\theta_k^+)$

$L^- = L(\theta_k^-)$

Gradient approximation:

$$\hat{g}_k = \frac{L^+ - L^-}{2c_k\Delta_k}$$

Parameter update:
$\theta_{k+1} = \theta_k - a_k\hat{g}_k$
Update coefficients:

$$a_k = \frac{a}{(k+1+A)^\alpha}$$

$$c_k = \frac{c}{(k+1)^\gamma}$$

Increment the iteration count k.

3. Convergence Check:
Repeat the iteration until convergence criteria are met (e.g., maximum iterations, tolerance threshold).

Implementation
Initialization

Choose initial values for θ_0 based on domain knowledge or preliminary experiments. Set the SPSA coefficients appropriately. Typical values are α=0.602, γ=0.101 and A=10 (tuning may be required).

Objective Function

Define the objective function (θ) L(θ) based on UAV performance metrics such as stability, control error, energy efficiency, etc.

Autonomous performance cost, longitudinal cost, weighted lateral cost, total cost and endurance coefficients are the weight values during the application of SPSA algorithm and are selected by considering all design parameters (autonomous performance cost vs. longitudinal cost vs. lateral cost). The weight values are determined according to the ratios of the design performance criteria in each iteration.

The SPSA algorithm offers an efficient and robust method for optimizing the control parameters of an eight-rotor UAV with a variable configuration. By adjusting the hub angle and PID coefficients, the UAV can achieve optimal performance across different operational scenarios. This approach ensures that the UAV maintains stability and control while transitioning between configurations, leveraging the flexibility provided by the unique design.

3. Result and Discussion

Hub angle and arm elevation angle changes were examined together for lateral and longitudinal flight. Flight simulation and calculations for longitudinal and lateral flight are set to 1 (degree). The cost index includes the terms longitudinal and lateral flight. To minimize the cost index, a combined approach combining longitudinal and lateral flight cost index was used instead of traditional methods. With the combined approach, the optimum values of the transformation

parameters are designed simultaneously for both the longitudinal and lateral flight control system. As a result, both PID coefficients and migration rates for longitudinal and lateral flight were determined separately for each iteration. SPSA is an iteration-based optimization algorithm. For this reason, the number of SPSA iterations was chosen as the optimum value of 10.

In order to obtain improvement in the autonomous performance of the multirotor and to keep the PID coefficients at better levels with lateral and longitudinal movements, multirotor control was performed with SPSA using transformation. In order to obtain at least 10-15% improvement in the multirotor autonomous performance index, the cost function given in equation 16 related to both lateral and longitudinal movements was created.

$$\%J_{tot_i} = J_{long_i} + \frac{J_{long_0}}{J_{long_0}} + J_{lat_i} \quad (16)$$

In the case where the lateral and longitudinal flight control system is handled with SPSA using transformation, $\frac{\pi}{2}$ for lateral flight and 1 degree for longitudinal flight are applied. SPSA determines seven parameters in the flight parameter determination phase. 1 of these is the transformation parameter, 3 of them are lateral flight PID coefficients and 3 of them are longitudinal flight parameters.

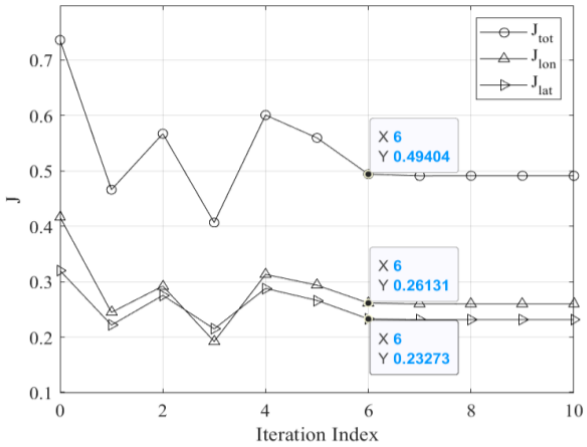

Figure 4. Cost Optimization; Total, Longitudinal, Lateral

In this study, PID coefficients in all simulations except optimization were given by using similar studies in the literature and past experiences. The PID coefficients used for longitudinal and lateral motion control are; 50,5,50.

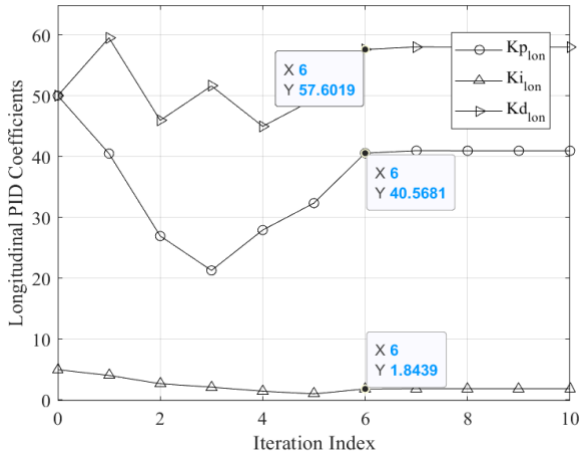

Figure 5. Longitudinal PID Coefficients

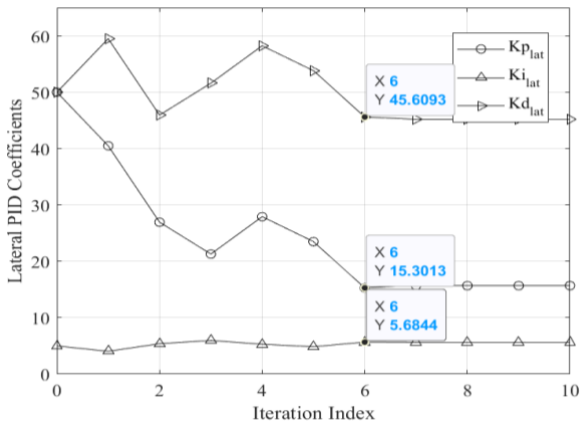

Figure 6. Lateral PID Coefficients

Design performance criteria were examined separately to achieve improvements in aircraft longitudinal and lateral flight autonomous performance. Design performance criteria provide precise information about the stability of a system (Oktay et al., 2017). In Figs. 10 and 11 the design performance criteria are presented for longitudinal and lateral flight. Longitudinal flight closed loop rise time, settling time and overshoot values are given in the graph below. SPSA has achieved improvement in system parameters in the 6th iteration compared to the initial values. Satisfactory results were obtained in other simulations. For this reason, it was limited to the 10th iteration and thus unnecessary calculations were not made and the workload of the system was reduced.

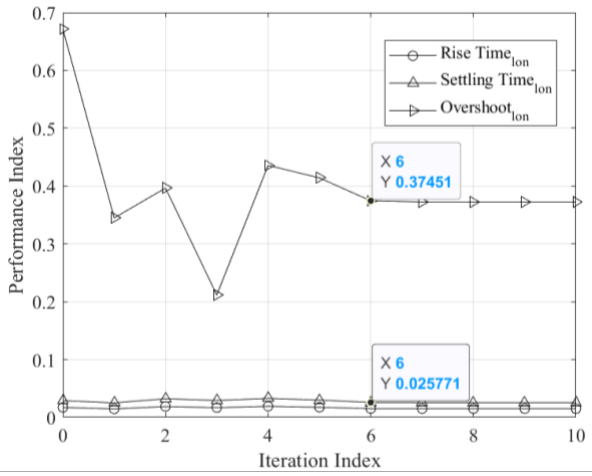

Figure 7. Longitudinal Performance Index

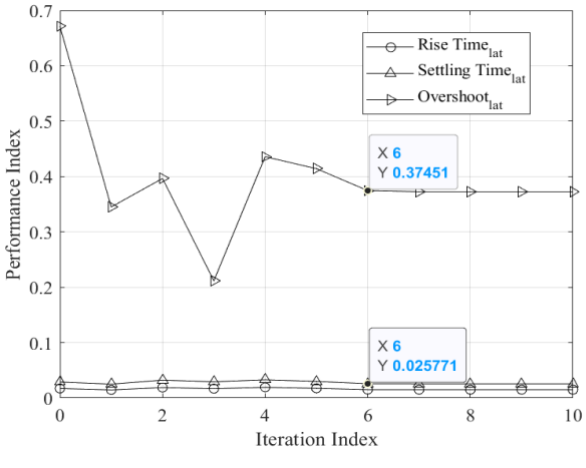

Figure 8. Lateral Performance Index

In the initial state, the hub angle (α) between the arms is 22.5 degrees, and as it increases to 45 degrees, the shape change narrows laterally and longitudinally.

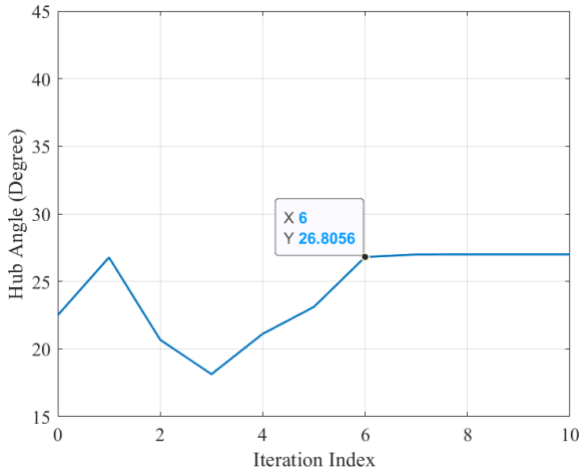

Figure 9. Hub Angle Values in Each Iteration

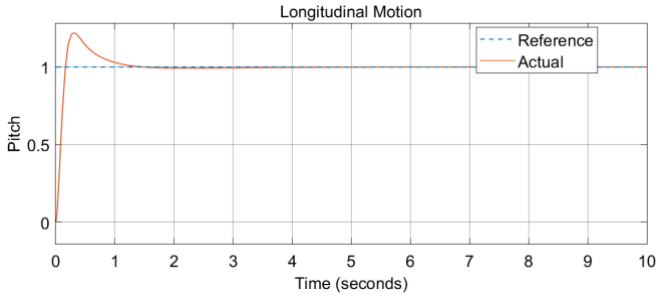

Figure 10. Pitch Angle Signal (Responses to Longitudinal Motion)

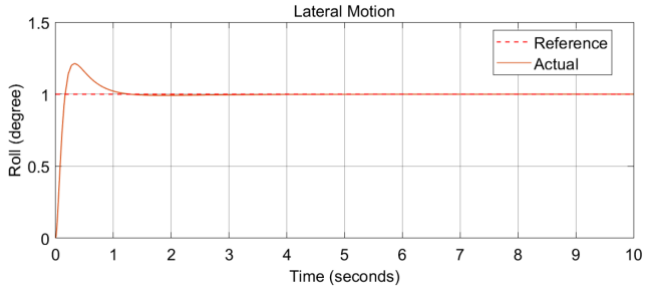

Figure 11. Roll Angle Signal (Responses to Lateral Movement)

Simulation results were compared with the initial values and are given in Table 3.

Table 3. Initial and Final Values of Variables in SPSA Optimization

Variable	Unit	Initial Value	Last Value
α	degree	22.5	26.8
$K_{Plongitudinal}$	-	50	40
$K_{Ilongitudinal}$	-	5	1.8
$K_{Dlongitudinal}$	-	50	57
$K_{Plateral}$	-	50	15
$K_{Ilateral}$	-	5	5.6
$K_{Dlateral}$	-	50	45
I_x	kgm^2	0.408	0.813
I_y	kgm^2	0.408	0.813
I_z	kgm^2	0.808	0.813

Performance criteria; Previous studies were examined and flight performance parameters (Trt, Tst, OS) were found to be satisfactory (Şahin et al. 2022).

Compared to similar studies (Köse, 2023) with the proposed combined approach, SPSA not only made optimum predictions without reaching the PID parameters at limit values, but also achieved the desired morphing rate quickly (Fabris et al., 2021)

4. Conclusion

This paper addresses the development of a control system model for both longitudinal and lateral flight under varying arm intersection angles. The Simultaneous Perturbation Stochastic Approximation (SPSA) optimization method was employed to determine optimal transformation parameters and to calculate the PID gains for longitudinal and lateral flight. The overall cost index demonstrated effective performance for both flight modes. Initially, the PID coefficients for both longitudinal and lateral flight were set at (50, 5, 50). After applying the SPSA method, the optimized PID coefficients for longitudinal flight were calculated as (40, 1.8, 57), and for lateral flight, as (15, 5.6, 45). These results indicate that the optimization method is effective, as it identifies optimal coefficients without reaching boundary values. As shown in Figures 5 through 9, the SPSA algorithm achieved optimal results by the 6th iteration.

The change in the arm intersection angle of the aircraft affects its dynamic model. The moment of inertia values obtained from analytical calculations and the aircraft model designed in the CATIA V5 software are presented in Table 2, showing consistency between the two methods. This consistency was achieved by integrating the analytical method into the SPSA optimization algorithm's framework. The equations and algorithm derived for the aircraft's controller design were simulated using the MATLAB/Simulink software with a state-space model. The hub angle was set at 26.8 degrees, with the best optimization result occurring in the 6th iteration, aligning with the expected performance of the SPSA algorithm.

Future studies will focus on developing a navigation system for indoor environments using image processing and artificial intelligence algorithms (Uzun et al., 2021). This system, combined with the proposed guidance algorithm, aims to achieve optimal autonomous flight in confined spaces.

Conflicts of Interest

The authors declare that there is no conflict of interest regarding the publication of this paper.

References

Alanezi, M.A., Haruna, Z.; Sha'aban, Y.A., Bouchekara, H.R.E.H., Nahas, M., Shahriar, M.S. (2022). Obstacle Avoidance-Based Autonomous Navigation of a Quadrotor System. Drones 6, 288.

Bao, X., Niu, Y., Li, Y., Mao, J., Li, S., Ma, X., Yin, Q., Chen, B. (2022). Design and Kinematic Analysis of Cable-Driven Target Spray Robot for Citrus Orchards. MPDI/Appl. Sci., 12, 9379.

Chen, S., Zhou, W., Yang, A.-S., Chen, H., Li, B., Wen, C.Y. (2022). An End-to-End UAV Simulation Platform for Visual SLAM and Navigation. MPDI/Aerospace, 9, 48.

Coban, S., Bilgic, H., Akan, E. (2020). Improving Autonomous Performance of a Passive Morphing Fixed

Wing UAV. Information Technology and Control, 49(1), 28-35.

Desbines, A., Expert, F., Boyron, M., Diperi, J., Viollet,S., Ruffier, F. (2017). X-Morf: A crash-separable quadrotor that morfs its X-geometry in flight. 2017 Workshop on Research, Education and Development of Unmanned Aerial Systems (RED UAS).

Fabris, A., Kleber, K.D., Falanga and Scaramuzza, D. (2012). Geometry-aware Compensation Scheme for Morphing Drones, 2021 IEEE International Conference on Robotics and Automation (ICRA), Xi'an, China, pp. 592-598.

Falanga, D., Kleber, K., Mintchev, S., Floreano, D., Scaramuzza, D. (2018). The Foldable Drone: A Morphing Quadrotor that can Squeeze and Fly. IEEE Robotics and Automation Letters. Preprint Version. Accepted November.

Husain, Z., Al Zaabi, A., Hildmann, H., Saffre, F., Ruta, D., Isakovic, A.F. (2022). Search and Rescue in a Maze-like Environment with Ant and Dijkstra Algorithms. MPDI/Drones, 6, 273.

Köse, O., (2023). Yapay Sinir Ağları, PID ve Başkalaşım ile Octorotor Yanal Uçuş Kontrolü . 4th International Black Sea Modern Scientific Research Congress (pp.79-90). Rize, Turkey

Köse, O., Oktay, T. (2019). Dynamic Modeling and Simulation of Quadrotor for Different Flight Conditions European Journal of Science and Technology, no. 15, pp. 132-142.

Köse, O., Oktay, T. (2021). Morphing with SPSA and ANN. Intelligent Systems and Applications in Engineering. Ijisae, 9(4), 159–164.

Oktay T., Uzun M., Çelik H., Konar M. (2017). Pid Based Hierarchical Autonomous System Performance Maximization of a Hybrid Unmanned Aerial Vehicle (Huav). Anadolu Univ. J. of Sci. and Technology A – Appl. Sci. and Eng. 18 (3)

Oktay, T., Sal, F. (2016). Combined passive and active helicopter main rotor morphing for helicopter energy save. Journal of the Brazilian Society of Mechanical Sciences and Engineering, 38(6), 1511-1525.

Şahin, H., Kose, O. and Oktay, T. (2022). Simultaneous autonomous system and powerplant design for morphing quadrotors, Aircraft Engineering and Aerospace Technology, Vol. 94 No. 8, pp. 1228-1241

Uzun, M., Özdemir, M., Yıldırım, Ç.V., Çoban, S. (2021). A Novel Biomimetic Wing Design and Optimizing Aerodynamic Performance. Journal of Aviation, 6(1), 12-25.

Zhang, Z., Li, X., Wang, X., Zhou, X., An, J., Li, Y. (2022). TDE-Based Adaptive Integral Sliding Mode Control of Space Manipulator for Space-Debris Active Removal. MPDI/Aerospace, 9, 105.

Cite this article: Ozen, E., Oktay, T. (2024). Maximization of Flight Performance of Eight-Rotor Multirotor with Differentiated Hub Angle. Journal of Aviation, 8(3), 206-213.